

1 Introduction

This report describes the numerical study on predicting the diffraction loads by a fixed Lewis form body in regular waves. The computations are performed by using the 2D-Numerical Wave Tank, which is the fully-nonlinear time domain simulation program originally developed by an author. The main purpose of this study is to confirm the validity of a numerical wave tank for the diffraction problem.

The Numerical Wave Tank (NWT) group of the International Society of Offshore and Polar Engineers was established at the 5th ISOPE conference in The Hague (1995). At the 7th conference on Honolulu (1997), it was decided by the member of the group to begin series of informal work shop meeting where computational benchmark cases will be defined and their results discussed and commented in a special session during the forthcoming ISOPE conference. A free access data bank will be created and enriched with the numerical results of the participants, so that the everybody can get data files and to perform his own analysis and comparison with any other participant. The 1st and the 2nd NWT Workshop session were held in ISOPE98 Montreal Conference and ISOPE99 Brest Conference. The problems and numerical results discussed in the previous workshop are already opened at the following Web site :

- <ftp://ftp.ec-nantes.fr/NWT/1998/>
- <http://www.srimot.go.jp/dyn/member/tanizawa/>

The 3rd NWT Workshop session will be held in ISOPE2000 Seattle Conference, where the topic is the diffraction force computation by numerical wave tanks and pressure computation on the body is the key point.

The benchmark cases assigned in the 3rd NWT Workshop are computed in this report. Numerical results are compared with the experimental results and theoretical results based on linear theory. Only the time-series data of simulated wave exciting forces and wave elevations in a tank, and the boundary values for one period in the periodically steady state, are requested and these data have been already submitted to the NWT Workshop.

2 Fully nonlinear numerical wave tank

2.1 Mathematical formulation

We consider the problem on diffraction of regular waves by a fixed Lewis Form body, as it is illustrated in Fig.1. Fluid density ρ , gravitational acceleration g and water depth h are used as units to nondimensionalize the problem only in this section. Assuming an inviscid, incompressible fluid and an irrotational flow, the fluid motion is specified by the velocity potential $f(x,y,t)$, which satisfies the Laplace equation within the fluid domain $W(t)$ with the boundary $G(t)$.

$$\nabla^2 f = 0 \quad \text{in } W(t) \quad (2.1)$$

The boundary $G(t)$ consists of the piston wave maker surface $G_p(t)$, the free surface $G_F(t)$, the Lewis form body surface G_L , the right-end wall in the tank G_w and the horizontal bottom G_B . As time changes, the boundary $G_F(t)$ changes both its shape and its position, and the boundary $G_p(t)$ does only its position, while the other ones do neither.

The velocity potential f satisfies the kinematic and dynamic conditions on the free surface. Neglecting the surface tension and choosing zero atmospheric pressure as a level, we can write these conditions in the following Lagrangian form:

$$\frac{D\mathbf{r}}{Dt} = \nabla f \quad \text{on } G_F(t), \quad (2.2)$$

$$\frac{Df}{Dt} = \frac{1}{2} |\nabla f|^2 - y \quad \text{on } G_F(t), \quad (2.3)$$

where \mathbf{r} is the position vector of the fluid particle on the free surface. On the other boundaries, the boundary conditions are expressed by the impermeability conditions for f as follows:

$$\frac{\partial f}{\partial n} = \begin{cases} u_p(t) & \text{on } G_p(t), \\ 0 & \text{on } G_L, G_w \text{ and } G_B, \end{cases} \quad (2.4)$$

where $u_p(t)$ denotes the velocity of the piston wave maker and n is inward normal direction of the boundary. Due to the motion of the wave maker, the free surface is changed from the rest to the new position $y=h(x,t)$. So the initial conditions are expressed by:

$$f(x,y,0) = h(x,0) = 0 \quad \text{on } G_F(0). \quad (2.5)$$

Thus the velocity field in the fluid domain can be formulated as the initial value-boundary

value problem for the velocity potential f . Then the free surface is a Dirichlet boundary where f is prescribed, while the others are Neumann boundaries where $\partial f/\partial n$ is prescribed.

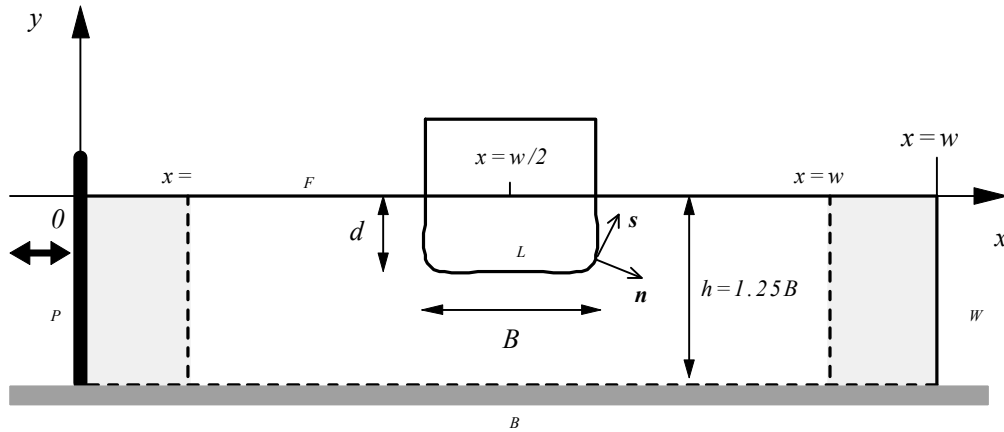


Fig. 1 Schematic view of numerical wave tank

The pressure acting on the body can be obtained using the nonlinear Bernoulli equation:

$$p = -f_t - \frac{1}{2} |\nabla f|^2 - y. \quad (2.6)$$

While ∇f can be computed from the solution of the velocity field, the acceleration field must be solved for the exact computation of f_t . As the more practical approach for the computation of f_t , the finite difference method can be applied. However, the problem such as numerical instabilities still remains in this case. Therefore, in this report, the boundary value problem for f_t as well as f is formulated and the direct solution procedure for f_t is considered.

The time derivative of the velocity potential f_t satisfies the Laplace equation in the fluid domain as well as the velocity potential f .

$$\nabla^2 f_t = 0 \quad \text{in } W(t) \quad (2.7)$$

The boundary condition for f_t on the Dirichlet boundary is expressed by

$$f_t = -\frac{1}{2} |\nabla f|^2 - y \quad \text{on } G_F, \quad (2.8)$$

while, on the Nuemann boundary, the boundary conditions can be written by the following forms:

$$\frac{\partial f_t}{\partial n} = \begin{cases} a_p(t) + \frac{\partial f}{\partial n} \frac{\partial^2 f}{\partial s^2} - \frac{\partial f}{\partial s} \frac{\partial^2 f}{\partial s \partial n} & \text{on } G_p, \\ \frac{\partial f}{\partial n} \frac{\partial^2 f}{\partial s^2} - \frac{\partial f}{\partial s} \frac{\partial^2 f}{\partial s \partial n} & \text{on } G_L, \\ 0 & \text{on } G_w \text{ and } G_B, \end{cases} \quad (2.9)$$

where $a_p(t)$ is the acceleration of the piston wave maker, $\partial/\partial s$ denotes tangential derivative on each boundary.

2.2 Numerical procedure

2.2.1 Solution by a higher order BEM

Applying the Green's second identity to the initial value boundary value problem, the boundary integral equation is obtained, which have the same form with respect to both f and f_t as follows:

$$c(P) f(P) = - \int_G \begin{Bmatrix} f(Q) \\ f_t(Q) \end{Bmatrix} \frac{\partial G(P,Q)}{\partial n_Q} dG(Q) + \int_G G(P,Q) \frac{\partial}{\partial n_Q} \begin{Bmatrix} f(Q) \\ f_t(Q) \end{Bmatrix} dG(Q) \quad (2.10)$$

where P is a point (x_p, y_p) on the boundary, Q an integral point (x_Q, y_Q) , and $c(P)$ the interior angle of the boundary at P . $G(P, Q)$ is the Green function for the two dimensional Laplace equation. Considering the mirror image of $G(P, Q)$ regarding the bottom boundary, the horizontal bottom boundary G_B can be excluded from the integration boundary G . Then $G(P, Q)$ is written as a form:

$$G(P, Q) = \frac{1}{2p} \ln \left(\frac{1}{r r'} \right), \quad (2.11)$$

$$\begin{cases} r = \sqrt{(x_p - x_Q)^2 + (y_p - y_Q)^2}, \\ r' = \sqrt{(x_p - x_Q)^2 + (y_p + 2h + y_Q)^2}. \end{cases}$$

A boundary element method (BEM) is used for the solution of the boundary integral equation (2.10). The following features are introduced in this work:

- Both the boundary geometry and the field function such as the velocity potential, its flux and so on, are discretized with the quadratic isoparametric elements for high accuracy.
- For the non-singular element where the observation point does not belong to the integrated element, a regular Gauss quadrature is used. On the other hand, for the singular element, a Gauss quadrature formula for the integrands with a logarithmic singularity is applied.
- On the intersection between the Dirichlet boundary and the Neumann boundary, the double nodes are placed. With the velocity potential continuous at this point, the velocity

of its intersection is deduced by taking into account the flux of the velocity potential on both boundaries. This leads to the advantage to avoid the numerical tangential derivative of f .

- The interior angle $c(P)$ is numerically computed by considering a particular Dirichlet problem where the uniform velocity potential value is imposed on the whole boundary.

It should be noted that those coefficients of the matrices which derive from the discretization of the equation (2.10) are in common for both cases between f and f_i . The solution procedure of the boundary value problem must be applied sequentially in time until the computation reaches the desired time. As the free surface boundary changes due to time evolution, the boundary condition also need to be updated corresponding with a new boundary, which is mentioned at the next section.

2.2.2 Time marching scheme

The initial value problem concerning the free surface is already formulated by (2.2)(2.3) (2.5). So the instantaneous geometry and the velocity potential can be computed by integrating the ordinary differential equations with respect to a time. The discretized forms of these equations are represented as follows:

$$\left. \begin{aligned} x_i(t+Dt) &= x_i(t) + Dt \frac{\partial f_i(t)}{\partial x}, \\ h_i(t+Dt) &= h_i(t) + Dt \frac{\partial f_i(t)}{\partial y}, \\ f_i(t+Dt) &= f_i(t) + Dt \frac{1}{2} \left[\left\{ \frac{\partial f_i(t)}{\partial x} \right\}^2 + \left\{ \frac{\partial f_i(t)}{\partial y} \right\}^2 \right], \\ (i=1,2,\dots,N_F) \end{aligned} \right\} \quad (2.12)$$

where $r_i=(x_i, h_i)$ is the fluid particles on the free surface, which is i th. node of total N_F nodes. The computation is performed according to following methods:

- The 4th order Runge-Kutta scheme is employed to integrate the ordinary differential equations.
- Auto time stepping algorithm is introduced to save a computational time.

Although a computation starts with an initially set time step size Dt , an current size is changed to a smaller size in case of violating the condition: $Dt \leq \text{Min} \{ Ds_i \} / \text{Max} \{ c_0 u_j \}$.

Ds_i denotes the element length defined by nodes $(i, i+1)$, u_j the velocity of j th node. The parameter c_0 is always set to 3.0 in present computations.

2.2.3 Artificial wave-absorbing zone and motion of wave maker

The artificial wave-absorbing zone is introduced at both ends of the tank as shown in Fig.1. The right absorbing zone works for absorbing incoming waves and preventing the reflection by the wall, while the left one works to pass the waves generated by the wave maker, but to absorb only the waves reflected by a body on the free surface and propagating toward the wave maker. Such an artificial wave-absorber can be made realized with additional numerical damping terms to the free surface conditions (2.2) (2.3), which are expressed as follows:

$$\frac{Dh}{Dt} = \frac{\partial f}{\partial y} - n(x)(h - h_{ref}) \quad \text{on } G_F(t), \quad (2.13)$$

$$\frac{Df}{Dt} = \frac{1}{2} |\nabla f|^2 - y - n(x)(f - f_{ref}) \quad \text{on } G_F(t), \quad (2.14)$$

where $n(x)$ is the damping coefficient:

$$n(x) = \begin{cases} aw \left(\frac{l-x}{l} \right)^2 & \text{for } x \leq l, \\ 0 & \text{for } l \leq x \leq w-l, \\ aw \left(\frac{x-w+l}{l} \right)^2 & \text{for } w-l \leq x. \end{cases} \quad (2.15)$$

In the definition of $n(x)$, w and l are angular frequency and wave length of incident wave respectively. The parameter a is the strength of damping and it is set as unit here. In the equations(2.13)(2.14), the artificial wave absorbing zone damps down the differences $h - h_{ref}$ and $f - f_{ref}$. The reference values are set to $h_{ref} = f_{ref} = 0$ and for using in front of the right-end wall, while these values about waves generated by the wave maker should be set to for using in case of the wave maker. In the present work, the solutions of propagating waves by linear theory are approximately used as both reference values.

$$\left. \begin{aligned} h(x,t) &= \frac{4A \sinh^2(kh)}{2kh + \sinh(2kh)} \cos(kx - wt), \\ f(x,y,t) &= \frac{4A \tanh(kh) \sinh(kh)}{w \{2kh + \sinh(2kh)\}} \cosh\{k(y+h)\} \sin(kx - wt), \end{aligned} \right\} \quad (2.16)$$

where A is a motion amplitude of the piston wave maker and k is the wave number of propagating waves generated by the wave maker.

In the present numerical wave tank, the motion $l_p(t)$ of the piston wave maker is expressed as follows:

$$\left. \begin{aligned} l_p(t) &= f(t) A \sin wt, \\ f(t) &= 1 - \exp(-t^2/25), \end{aligned} \right\} \quad (2.17)$$

where the time-function $f(t)$ makes it possible for the motion to start from the rest and increase gradually. In case of this time-function, it takes about three periods to reach the steady state.

2.2.4 Regridding and smoothing technique

The regridding every some time steps is carried out in simulating, which is one of successful technique for a long time simulation and also important from a viewpoint of simulating with high accuracy. For some nodes located near a wave maker moves rapidly toward a downstream direction especially in case of generating waves with a large amplitude motion, which leads to poor accuracy. In the present numerical wave tank, some grid systems are supplied, such as a grid system to make each element length equal and one to control the nodal density based on the geometrical curvature or the velocity of the node. The appropriate grid system can be chosen from them according to problems. Furthermore, the smoothing technique based on polynomials or B-spline also can be employed. This is effective to remove the numerical instability such as saw-toothed instability and so high frequency components in waves.

3 Numerical simulations

3.1 Description of case study

The numerical simulation is started from the calm condition at time $t=0$, and continued until the wave field converges to the periodically steady state. Computational conditions are as follows:

- Depth of the body : $d = B/2$
- Lewis form parameter : $H_0 = S = 1.0$
- Depth of wave tank : $h = 1.25 B$
- Amplitude of wave maker : $A/h = 0.015, 0.025, 0.035$
- Oscillating frequency of wave maker : $KB \left[= w^2 B/g \right] = 0.5, 1.0, 1.5, 2.0, 2.5, 3.0$
- Tank size : $w = 6l$, and the length of effective wave tank = $4l$

Totally 18 cases are simulated by changing amplitude (three kinds) and frequency (six kinds).

Table .1 computational size and set parameter

Test case		Number of Nodes				$\Delta t / T$	Regridding	Smoothing	CPU Time [s]
A/h	KB	N_p	N_F	N_L	N_w				
0.015	0.5	11	94	41	11	15	B/10	A/10	1334
	1.0	11	94	41	11	15	B/10	A/10	1320
	1.5	11	94	41	11	15	B/10	A/10	1207
	2.0	11	94	41	11	15	B/10	A/10	1163
	2.5	11	94	41	11	15	B/10	A/10	1393
	3.0	11	94	41	11	15	B/10	A/10	1143
0.025	0.5	11	94	41	11	20	B/10	A/10	1786
	1.0	11	94	41	11	20	B/10	A/10	1606
	1.5	11	94	41	11	20	B/10	A/10	1618
	2.0	11	94	41	11	20	B/10	A/10	1521
	2.5	11	90	41	11	20	B/10	A/10	1731
	3.0	11	78	41	11	20	B/10	A/10	1495
0.035	0.5	11	94	41	11	30	B/10	A/10	2412
	1.0	11	94	41	11	30	B/10	A/10	2405
	1.5	11	94	41	11	30	B/10	A/10	2416
	2.0	11	82	41	11	30	B/15	A/10	2087
	2.5	11	78	41	11	30	B/10	A/10	1938
	3.0	11	78	41	11	30	B/15	A/10	2147

(Regridding : A. no regridding, B. equal length, C. due to curvature, D. due to velocity)
 Smoothing : A. 5points formula by polynomials, B. by smoothing spline
 CPU : Celeron 366 MHz

3.2 Diffraction of regular waves by a fixed body

All computations are carried out for 30 period when the wave field is recognized as periodically steady state. The computational size and the parameters set in simulations are shown in Table.1. The wave profiles in the numerical wave tank are shown in from Fig.4 to Fig.9. Four kinds of wave profiles correspond with states at $t = (29+T/4)$, $(29+2T/4)$, $(29+3T/4)$ and $30T$, respectively. The wave diffraction is visible in these figures, ie, long waves transmit to the lee-side of the body, while short waves are almost reflected by the body. The situation close to standing waves is reached for high frequency's cases. At three positions ($x=1.75l$, $x=2.0l$ and $x=4.0l$) in the tank, the wave elevations are numerically measured. The time series of wave elevations at weather-side of the fixed body are shown as Fig.10, Fig.11 and Fig.12.

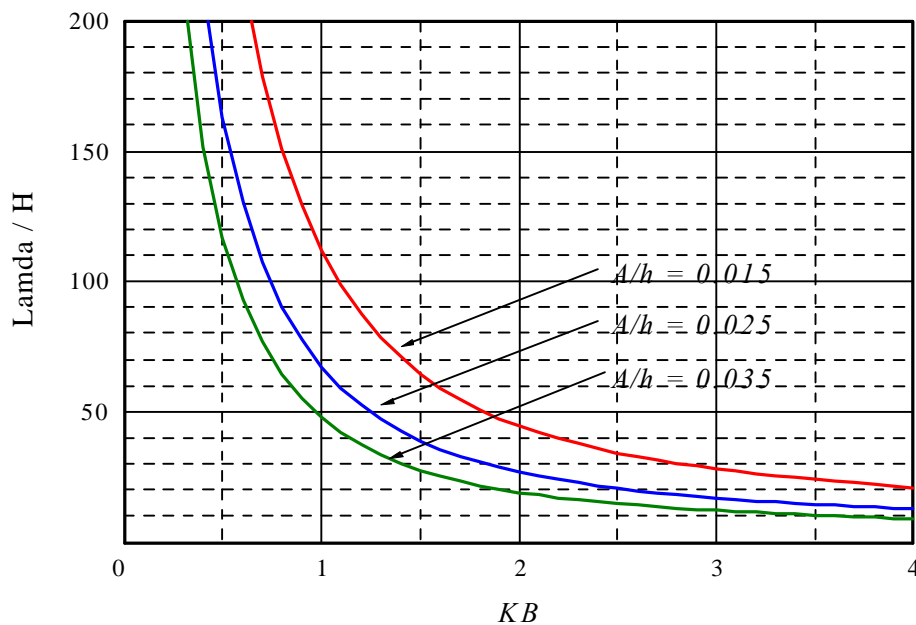


Fig.2 Wave steepness of propagation waves for infinite depth by linear theory

Fig2 illustrates wave steepness of a propagating wave generated by a piston wave maker, which is based on linear theory for deep water waves. In all present simulations, the steepest case is $H/l \approx 1/12$. The simulated time series of sway exciting force F_S (horizontal wave-exciting force), heave exciting force F_H (vertical wave-exciting force) and roll exciting moment M_R (wave-exciting moment) acting on a fixed Lewis form body, are shown in from Fig.13 to Fig.21. As incident waves' amplitude increases, the strong non-linearity can be exposed. Concerning cases with the strongest non-linearity in present simulations, each component of wave-exciting forces is compared in Fig.3. Although the wave profile with double crests for one period is one of non-linear characteristics, the hydrostatic component causes such a wave deformation in case of sway exciting force, while the hydrodynamic component itself does in case of heave exciting force.

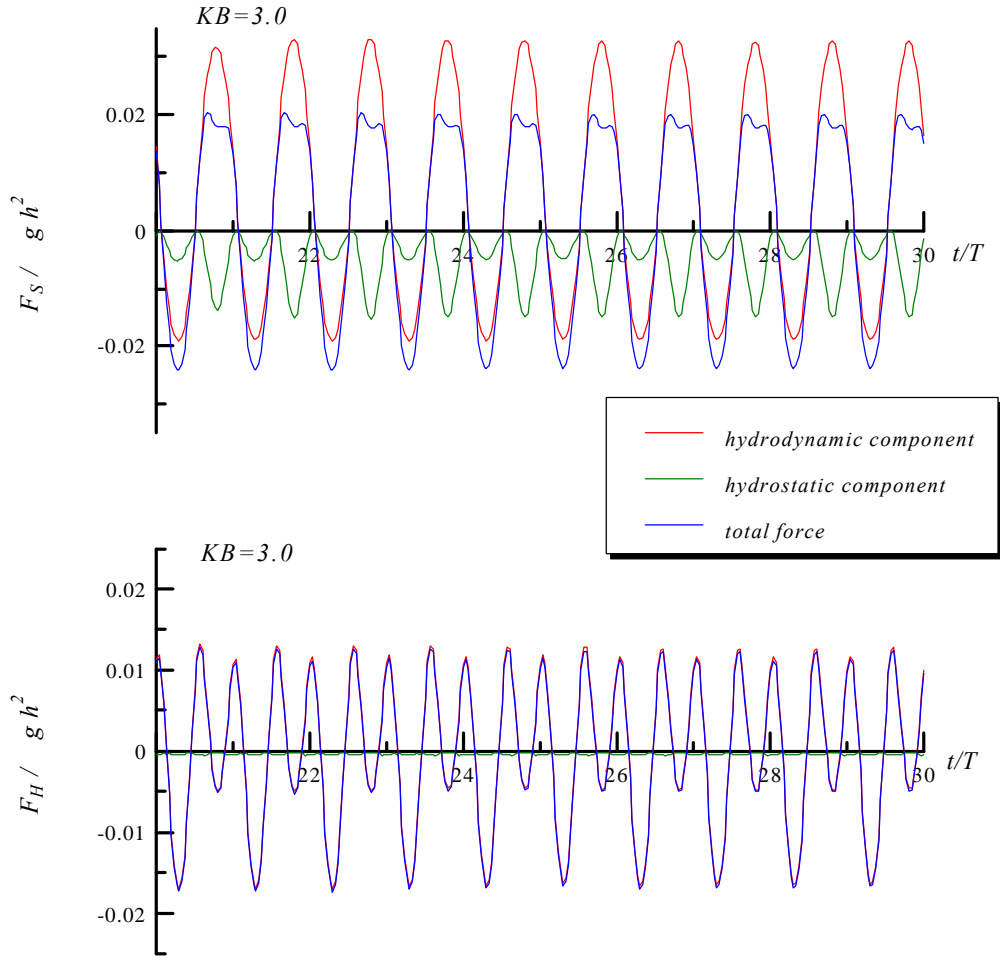


Fig.3 The component of wave exiting force , $A/h = 0.035$.

In the numerical wave tank, the force and the moment acting on a body can be computed as follows:

$$\left. \begin{aligned} F_S &= -\int_{G_L} p n_x ds, \\ F_H &= -\int_{G_L} p n_y ds, \\ M_R &= -\int_{G_L} p (x n_y - y n_x) ds, \end{aligned} \right\} \quad (3.1)$$

where (n_x, n_y) denotes normal vector \mathbf{n} on a body surface. p is the pressure expressed by equation (2.6). The hydrodynamic and hydrostatic components in Fig.3 mean the integration of pressure p_d and p_s components respectively.

$$\left. \begin{aligned} p_d &= -r \left[f_t + \frac{1}{2} |\nabla f|^2 \right], \\ p_s &= -r g y \quad . \end{aligned} \right\} \quad (3.2)$$

The buoyancy of a body in calm water is excluded from the heave force F_H in (3.1). So the hydrostatic pressure p_s in (3.2) means what the change of instantaneous free surface causes.

The frequency characteristics of these wave-exciting forces are shown in Fig.22, Fig.23 and Fig.24. To evaluate these time series data by a numerical wave tank, the Fourier analysis is employed by using only data for 5 periods in each time history between Fig.13 and Fig.21. This is just like analysis for experimental data. All results by the numerical wave tank are compared with the experimental results and the prediction by linear theory, although the conditions of water depth are different each other. Experimental data by Nojiri and Murayama (1975) are quoted from in the present study. As to the prediction by linear theory, the solutions of the radiation problem for deep water waves can be applied to the solutions of the present diffraction problem with the Haskind-Newman's relation. Then the wave-exciting forces for sway, heave and roll mode are expressed as follows:

$$\left. \begin{aligned} F_S &= -\frac{2irg}{k} n_0 a_I \bar{A}_S e^{-i(\omega t + e_S)} , \\ F_H &= \frac{2irg}{k} n_0 a_I \bar{A}_H e^{-i(\omega t + e_H)} , \\ M_R &= \frac{2irg}{k} n_0 a_I \left(\frac{B}{2} \right) \bar{A}_R e^{-i(\omega t + e_R)} , \end{aligned} \right\} \quad (3.3)$$

where n_0 represents an effect of finite water depth with a following form and it tends to $1/2$ as $h \rightarrow \infty$.

$$n_0 = \frac{1}{2} \left(1 + \frac{2kh}{\sinh(2kh)} \right) \quad (3.4)$$

In (3.3), \bar{A} and e are, respectively, the amplitude ratio and the phase difference between the body's motion and the radiation wave, and suffix letters S , H and R correspond with sway, heave and roll mode, respectively. These values are computed by using, it is called, the Ursell-Tasai method, which is a multi-pole expansions method. Between computational results by the numerical wave tank and by linear theory, the apparent differences can be recognized specially in low frequency. This is because the effect of water depth appears in computations. In case of a computation for larger h/B , it can be confirmed that the computation by the numerical wave tank shows a good agreements with the linear theory, even though it is a computation for a small KB value. Although the wave-exciting forces are nonlinear as shown in Fig.3, it does not give significant effects to the prediction of the first order forces. It should be, however, noted that the harmonics components of wave-exciting forces are substantial in some cases.

The incident waves, the reflected waves and the transmitted waves can be computed from time series of wave elevations simulated in the numerical wave tank. The reflection and the transmission coefficients are shown with experimental results in Fig.25. Considering that condition $a_I^2 = a_R^2 + a_T^2$ which comes from the assumption that the averaged energy flux is zero, the results by the numerical wave tank are more reasonable than the experimental ones. On the other hand, the amplitudes of the reflected wave and the transmitted wave can be written by using e in (3.3) as follows:

$$\left. \begin{aligned} a_R/a_I &= \text{Re} \left[-(\cos^2 e_H - \sin^2 e_S) + i(\cos e_H \sin e_H + \cos e_S \sin e_S) \right] , \\ a_T/a_I &= \text{Re} \left[1 - (\cos^2 e_H + \sin^2 e_S) + i(\cos e_H \sin e_H - \cos e_S \sin e_S) \right] . \end{aligned} \right\} \quad (3.5)$$

Some comparisons of the wave-drift force acting on the fixed Lewis form body is represented in Fig.26. As for the linear theory, the wave-drift force is expressed as follows:

$$F_D = \frac{1}{4} \left(1 + \frac{2kh}{\sinh(2kh)} \right) \rho g (a_I^2 + a_R^2 - a_T^2) \quad (3.6)$$

$$= n_0 \rho g a_R^2 \quad (3.7)$$

Two kinds of predictions by the numerical wave tank are show in Fig.26. One is based on the direct pressure integral method where the wave-drift force is computed as a time-averaged value of simulated sway exciting force. The other is by using equation (3.7) with the waves simulated by the numerical wave tank, which means partly applying the results of the first-order quantity predicted by the NWT. Although the effects of finite water depth seem to be demonstrated in case of the direct pressure integral method, the computational accuracy should be improved. To avoid the errors caused by non-dimensionalizing, the drift force dimensionalized by constants and the amplitude of incident wave are exhibited in Fig.27 and Fig.28. The wave-drift force is not proportional to the square of the incident wave in high frequency. In case that both KB value and wave steepness are large, the computational accuracy of drift force itself seems to be lost. As to the point that the wave-drift forces in Fig.26 in case of small A/h show lower values, this is partly because the hydrostatic components make a time averaged value smaller as shown in Fig.3. As the wave height gets larger and larger, the performance of artificial wave-absorbing zone is expected to be lower especially for the wave-absorbing zone in front of a wave maker, because the reference values to absorb waves are set to be equal to linear solutions. Since it is desirable to make the numerical wave tank size small from a viewpoint of saving computational times, the development of a wave-absorber is needed. Moreover, the more studies should be added to about predicting the wave-drift forces by the direct pressure integral method.

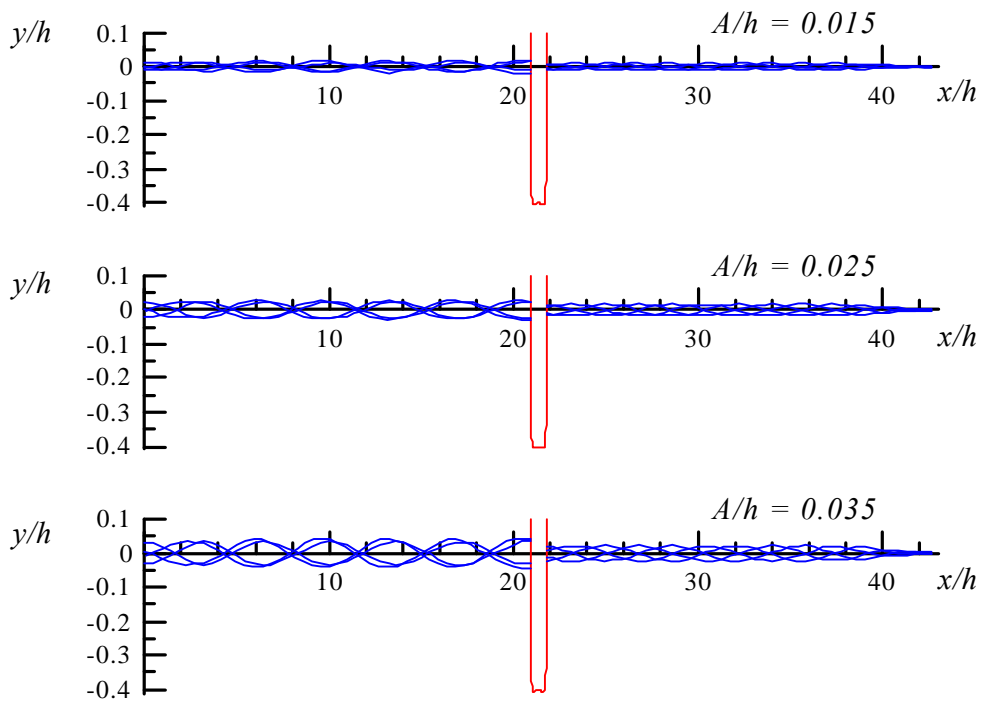


Fig.4 Wave profiles in the numerical wave tank, $KB = 0.5$

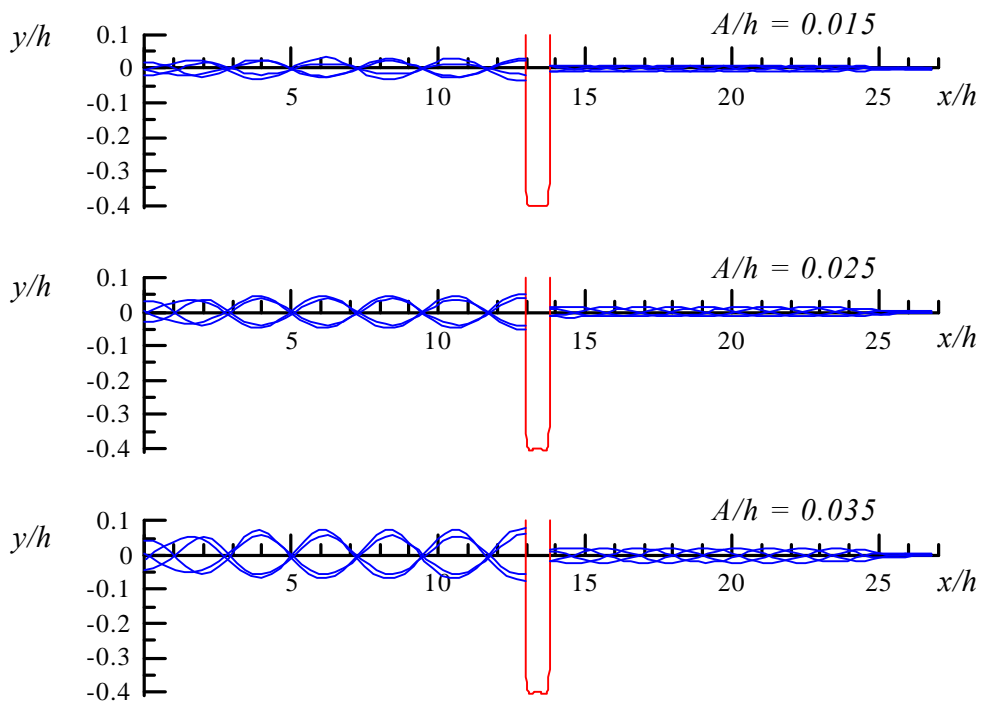


Fig.5 Wave profiles in the numerical wave tank, $KB = 1.0$

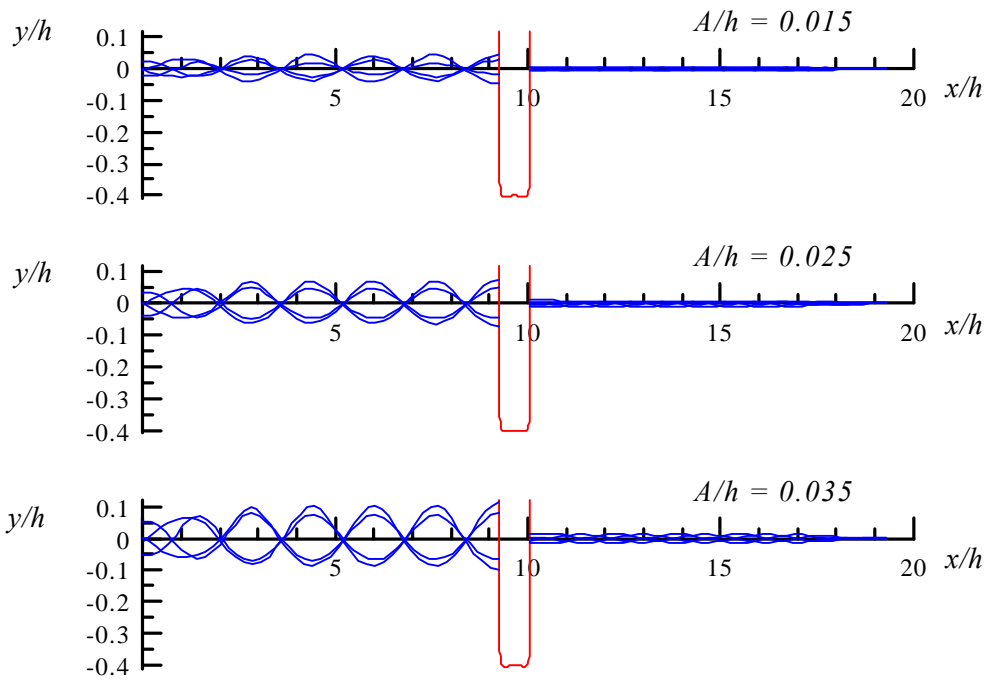


Fig.6 Wave profiles in the numerical wave tank, $KB = 1.5$

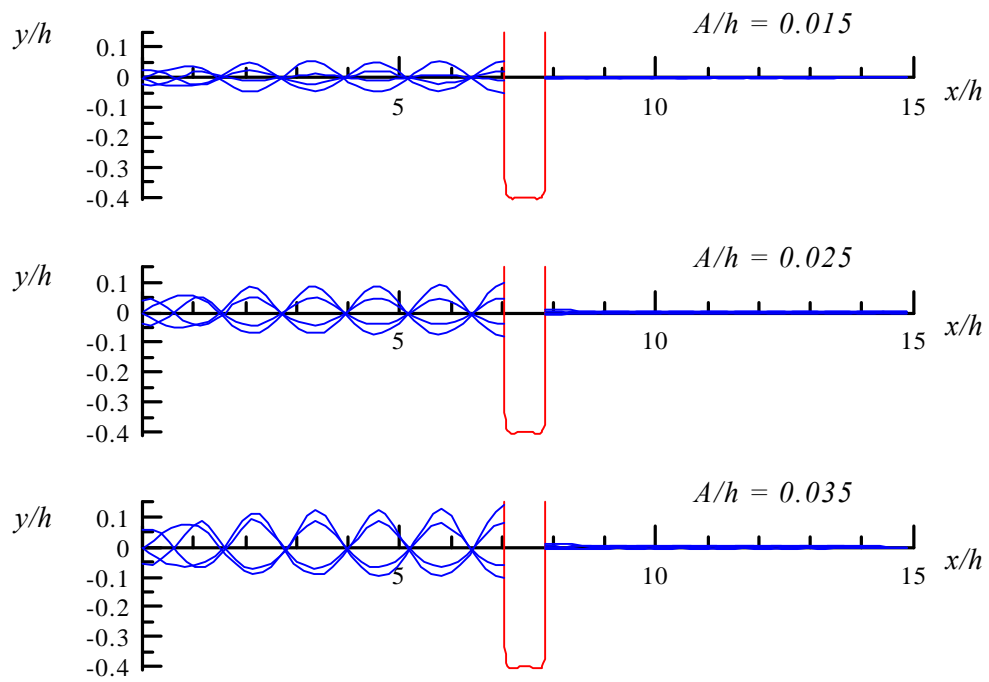


Fig.7 Wave profiles in the numerical wave tank, $KB = 2.0$

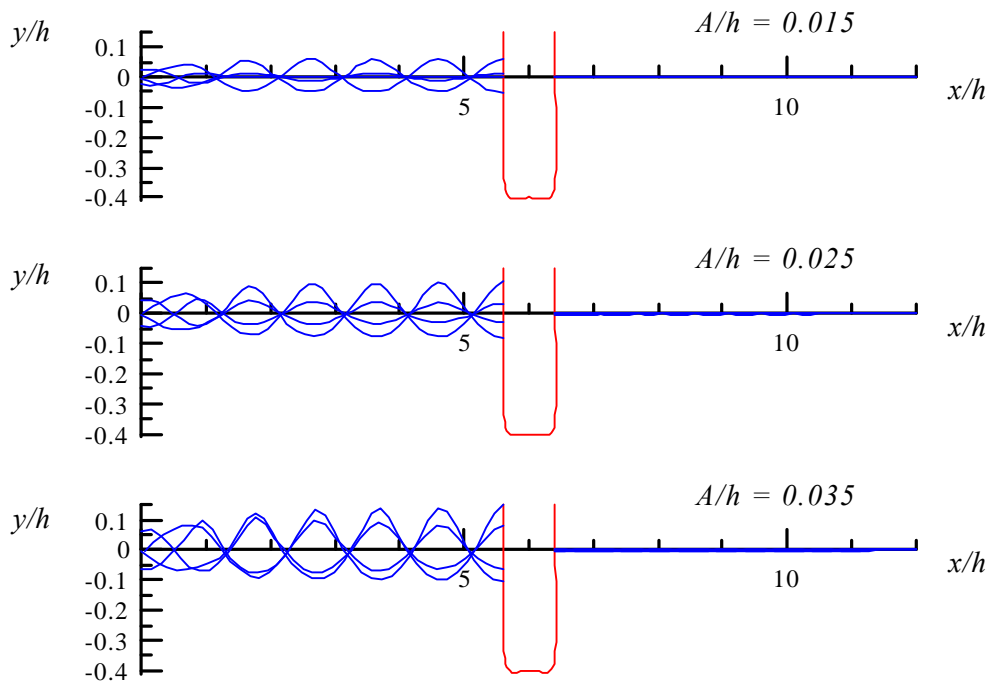


Fig.8 Wave profiles in the numerical wave tank, $KB = 2.5$

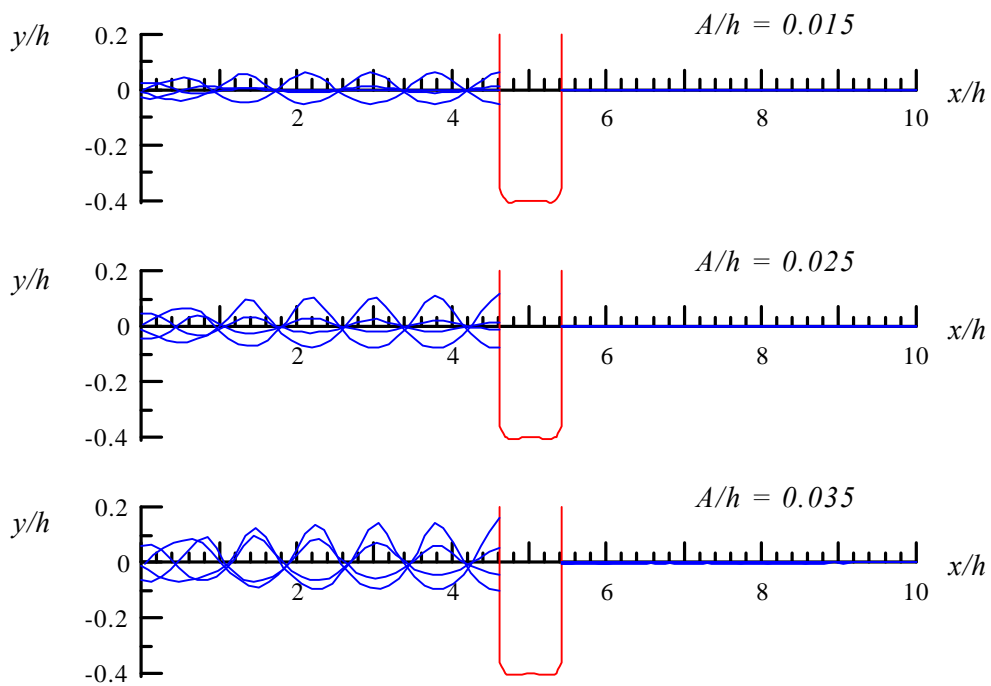


Fig.9 Wave profiles in the numerical wave tank, $KB = 3.0$

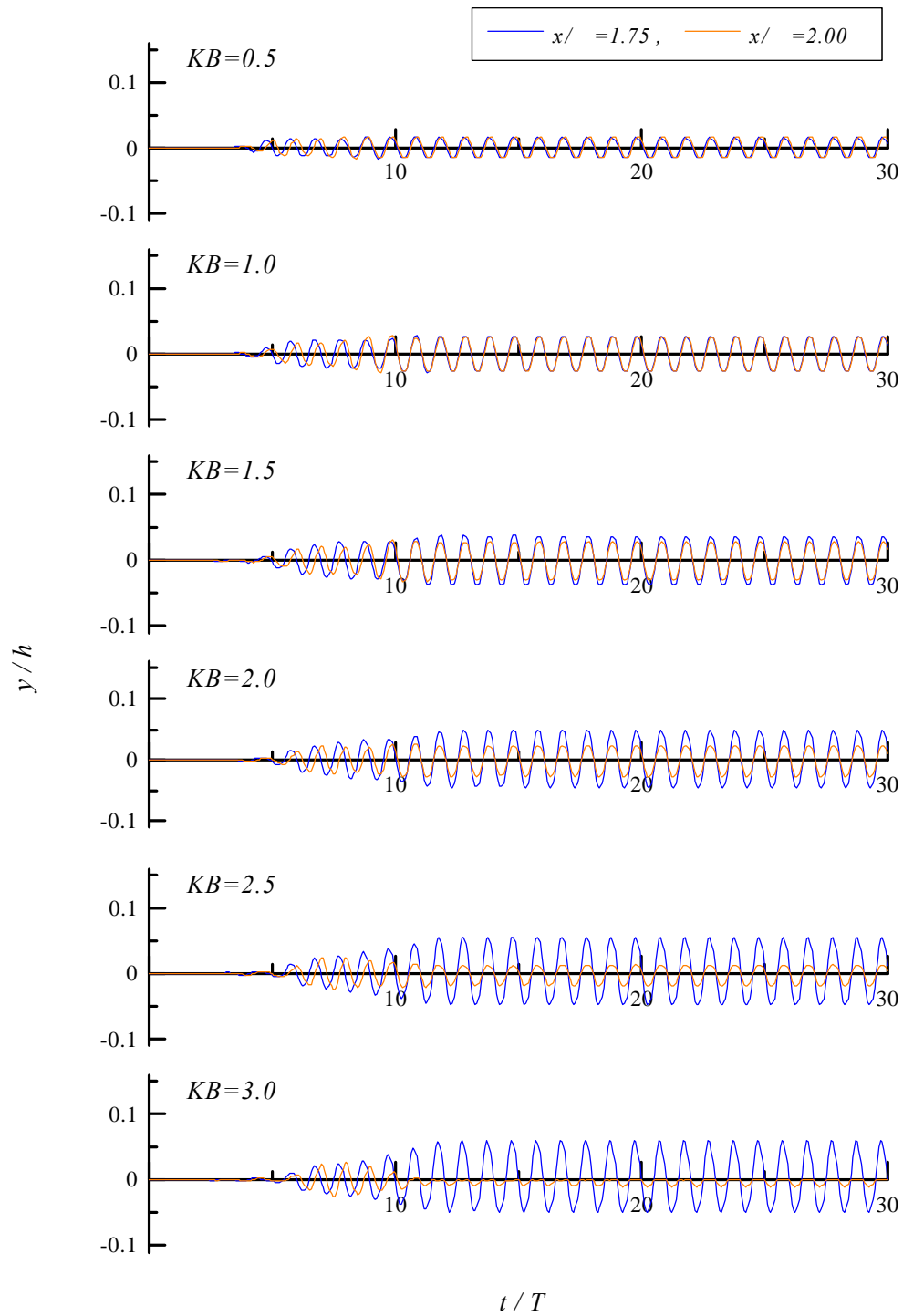


Fig.10 Wave elevations, $A/h=0.015$.

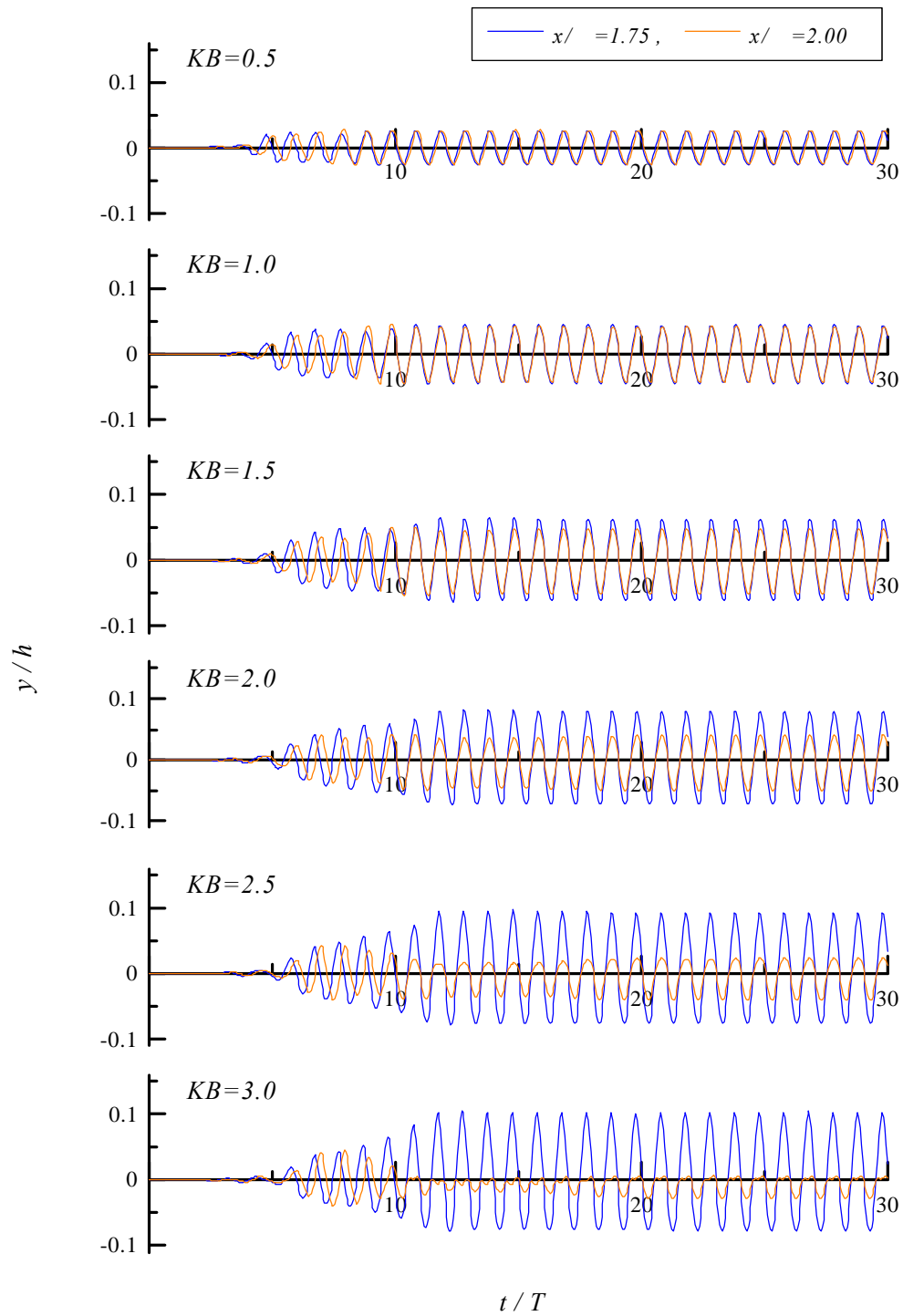


Fig.11 Wave elevations, $A/h=0.025$.

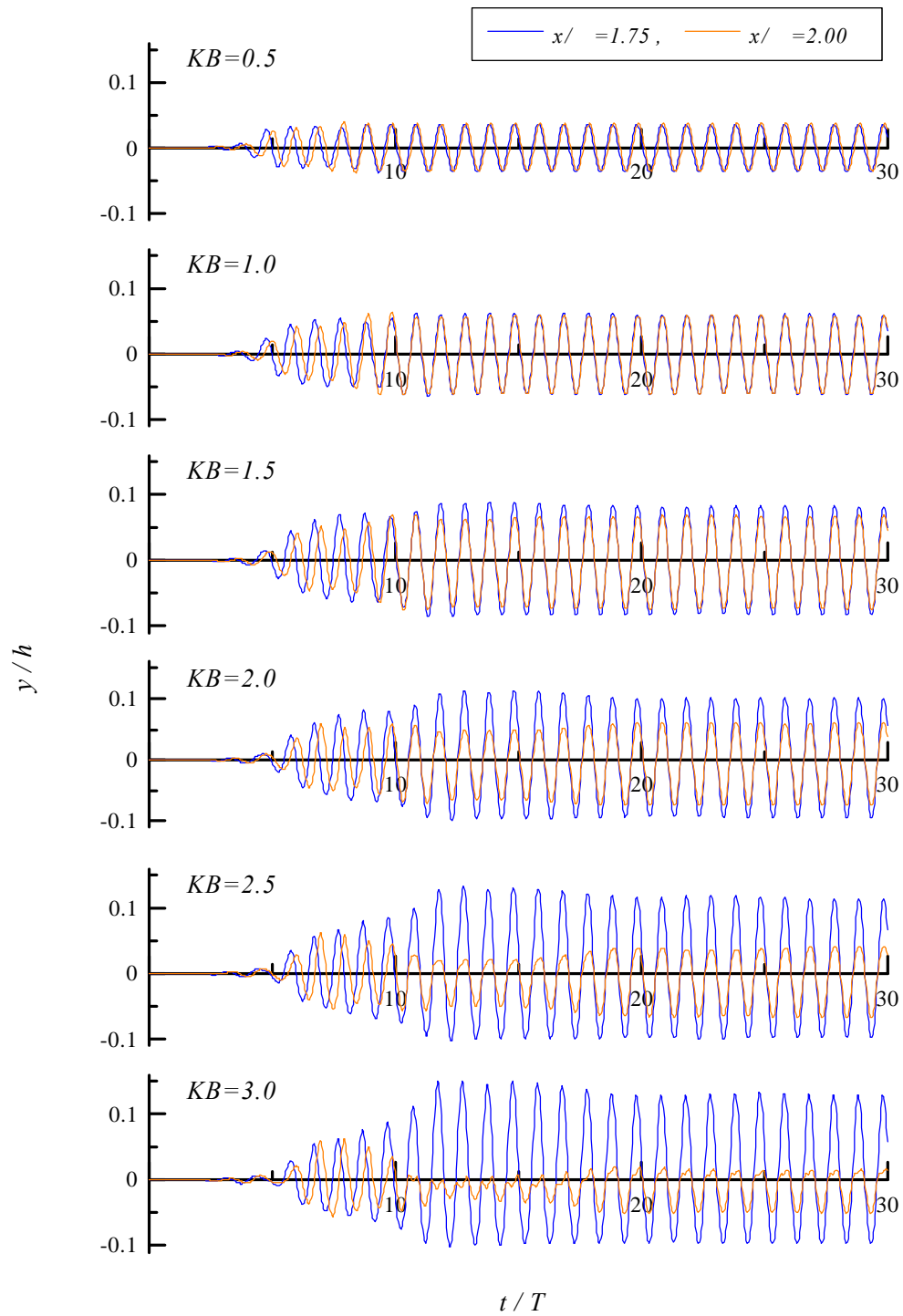


Fig.12 Wave elevations, $A/h=0.035$.

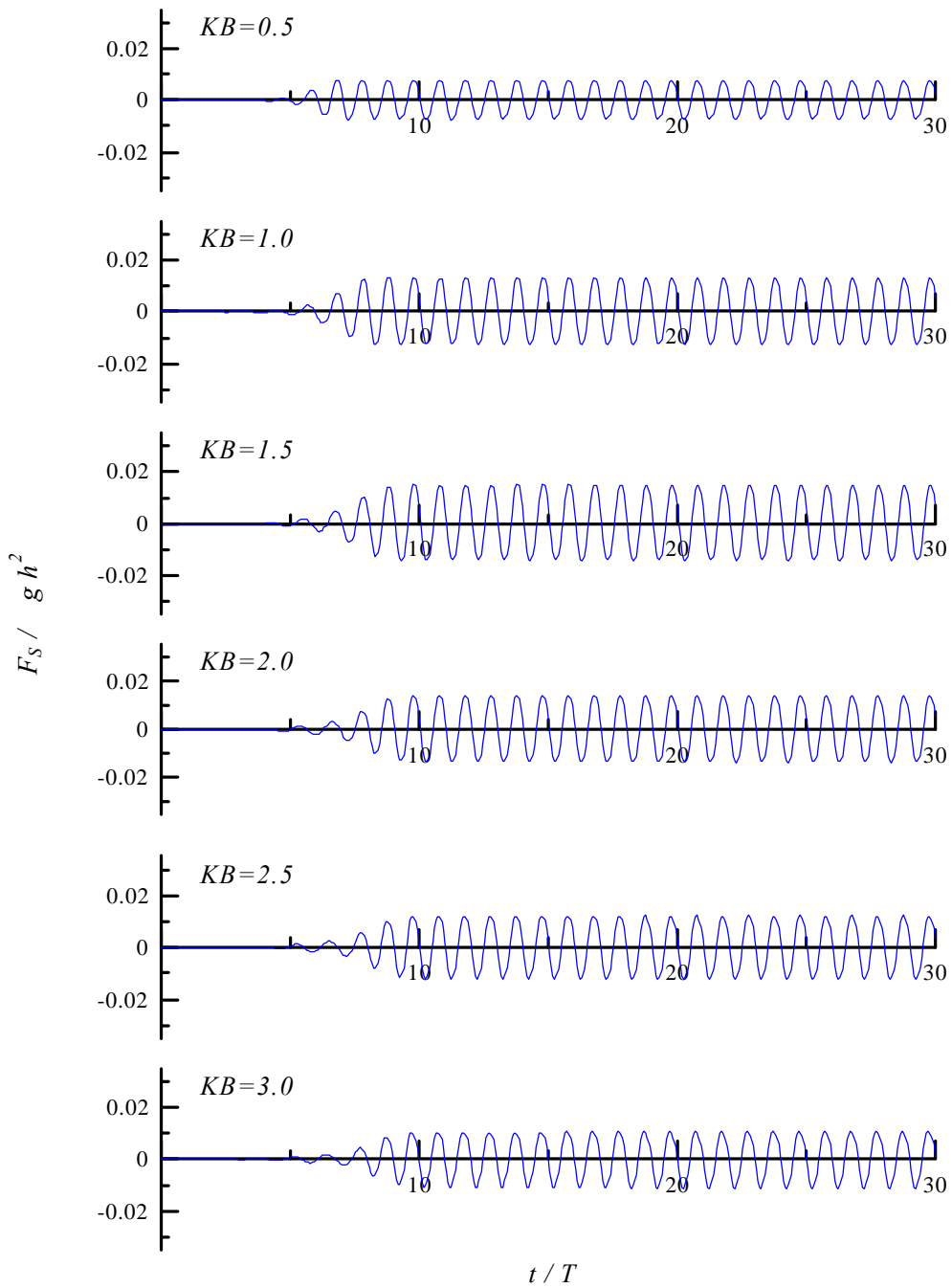


Fig.13 Simulated time series of sway exciting force acting on a fixed Lewis form body, $A/h = 0.015$.

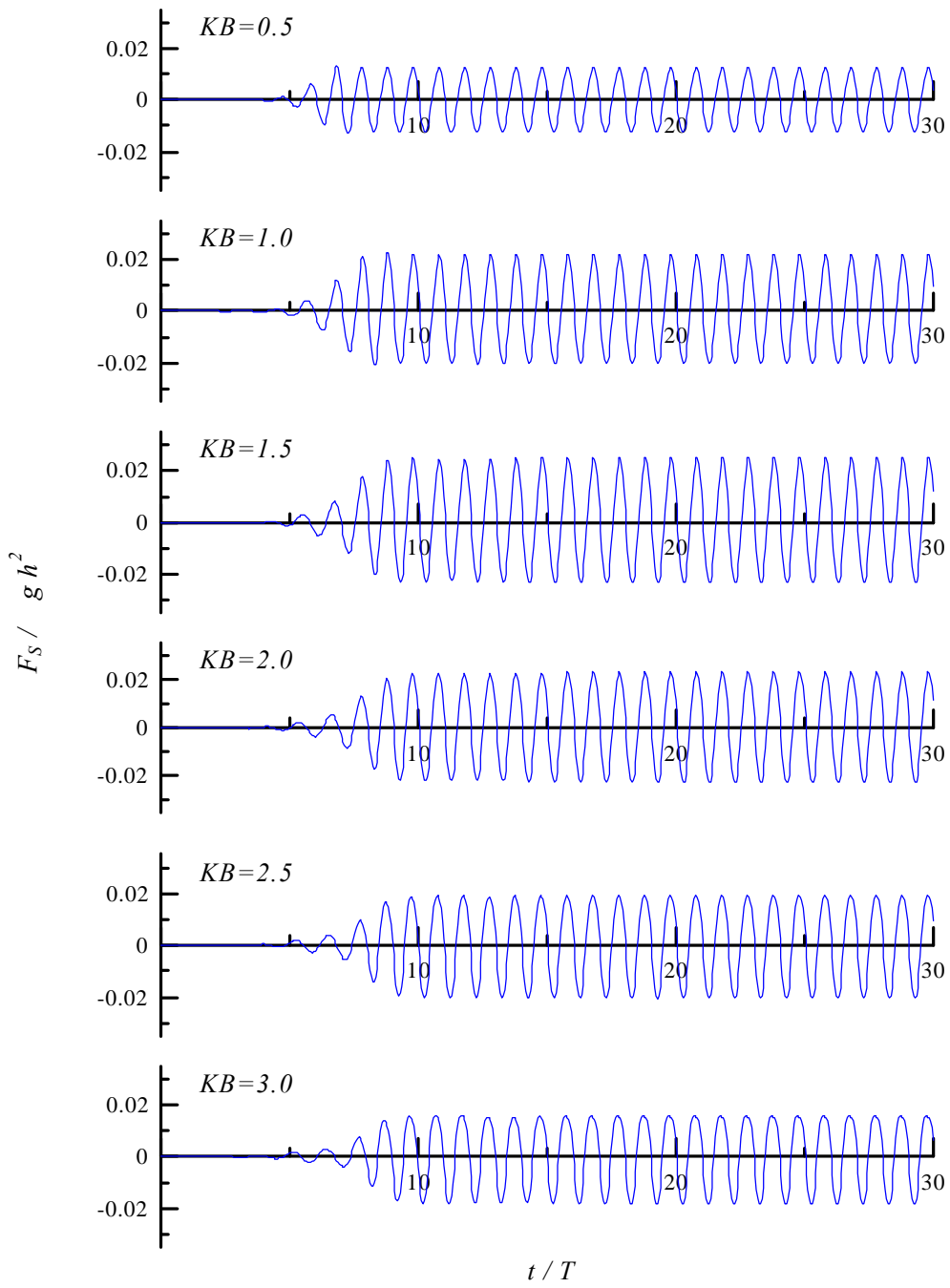


Fig.14 Simulated time series of sway exciting force acting on a fixed Lewis form body, $A/h = 0.025$.

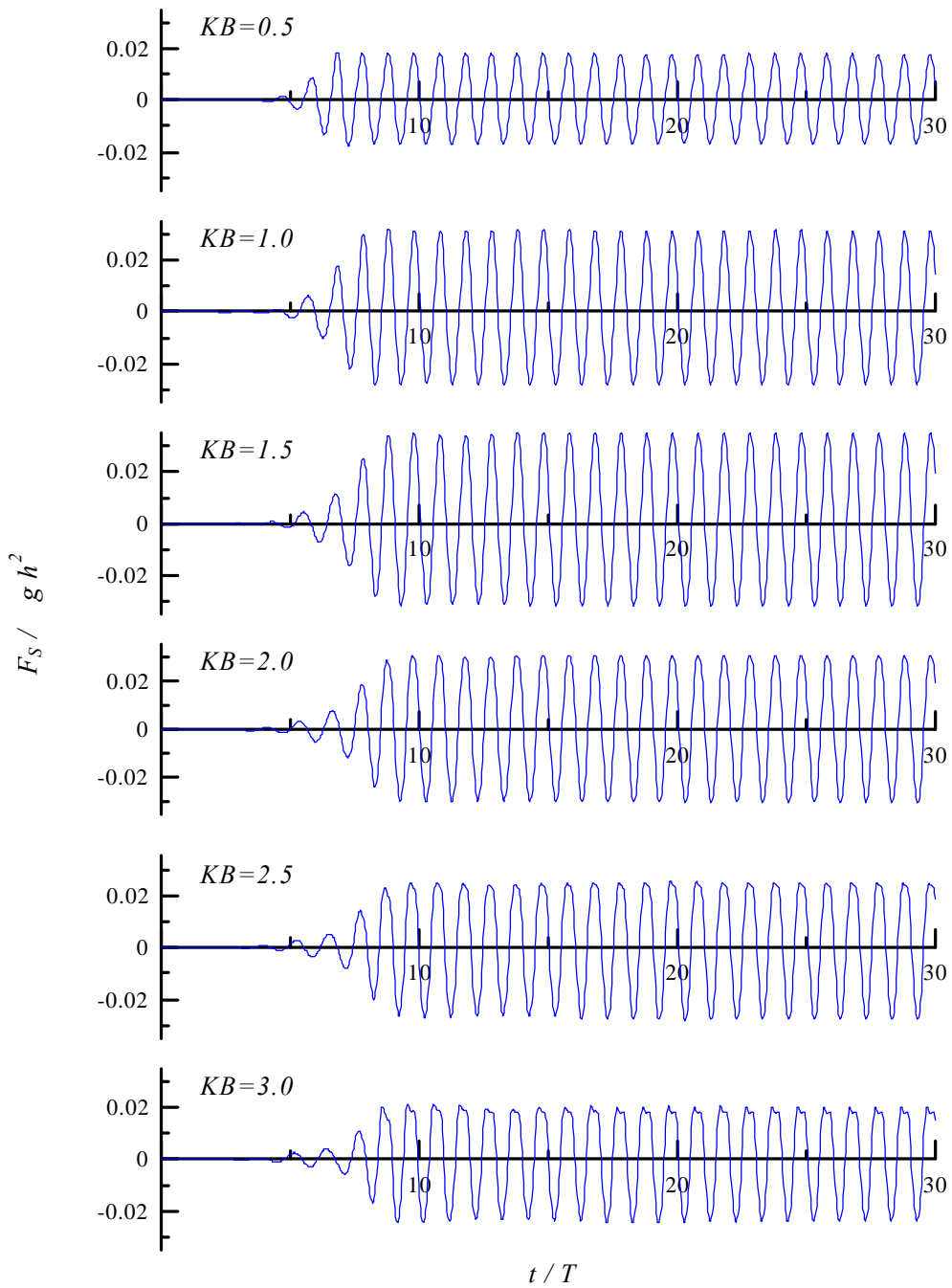


Fig.15 Simulated time series of sway exciting force acting on a fixed Lewis form body, $A/h = 0.035$.

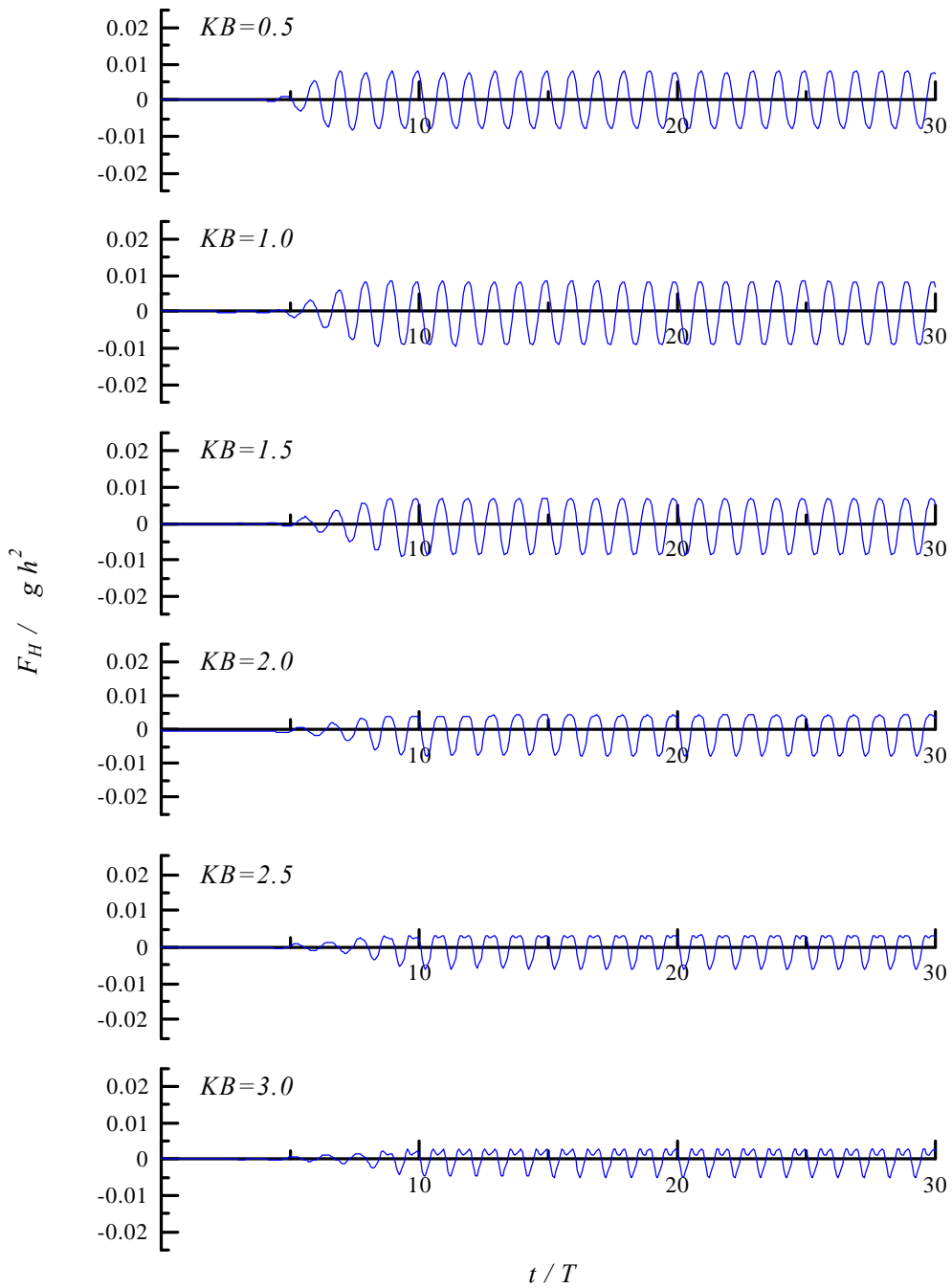


Fig.16 Simulated time series of heave exciting force acting on a Lewis form body, $A/h = 0.015$.

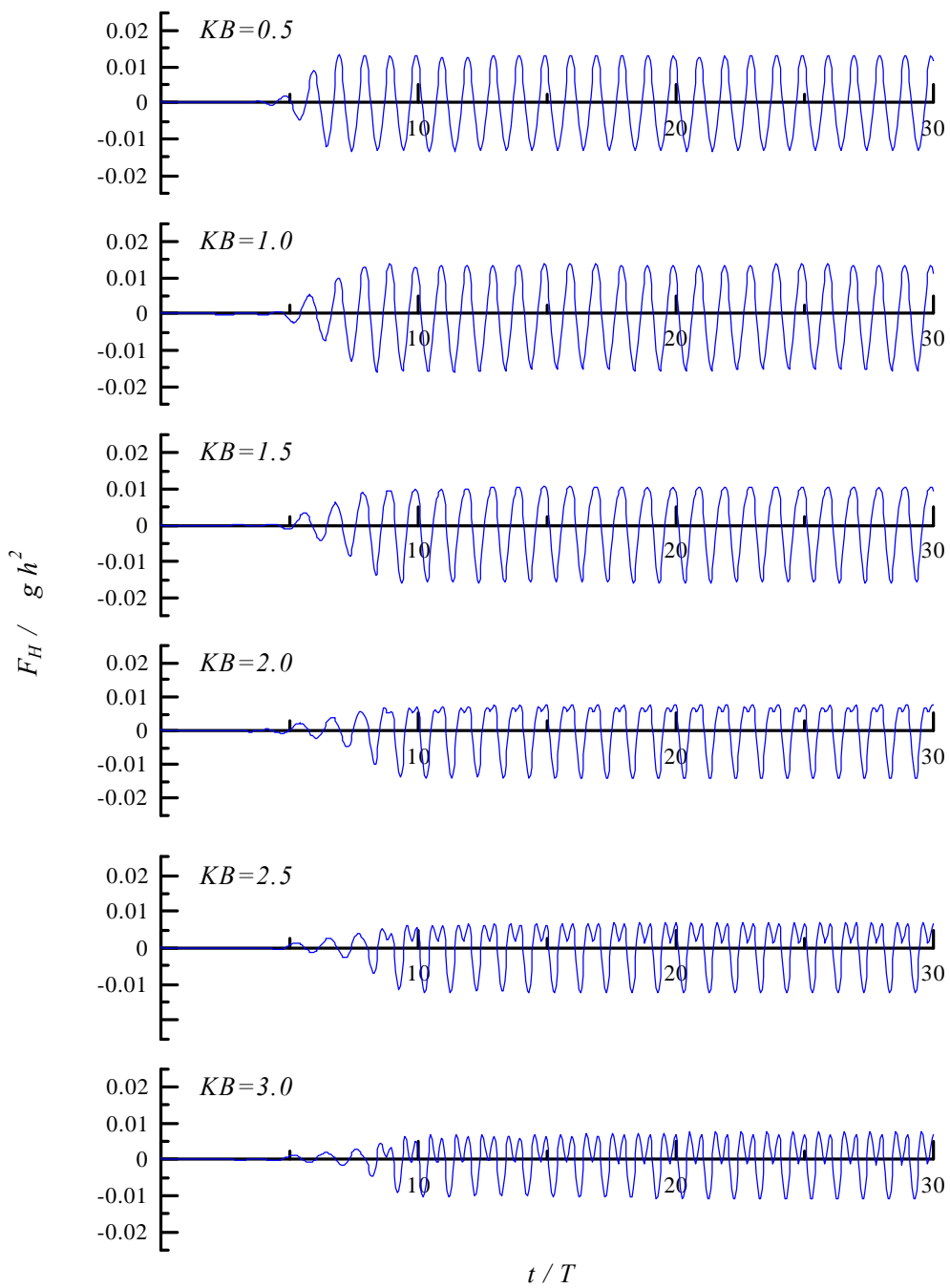


Fig.17 Simulated time series of heave exciting force acting on a fixed Lewis form body, $A/h = 0.025$.

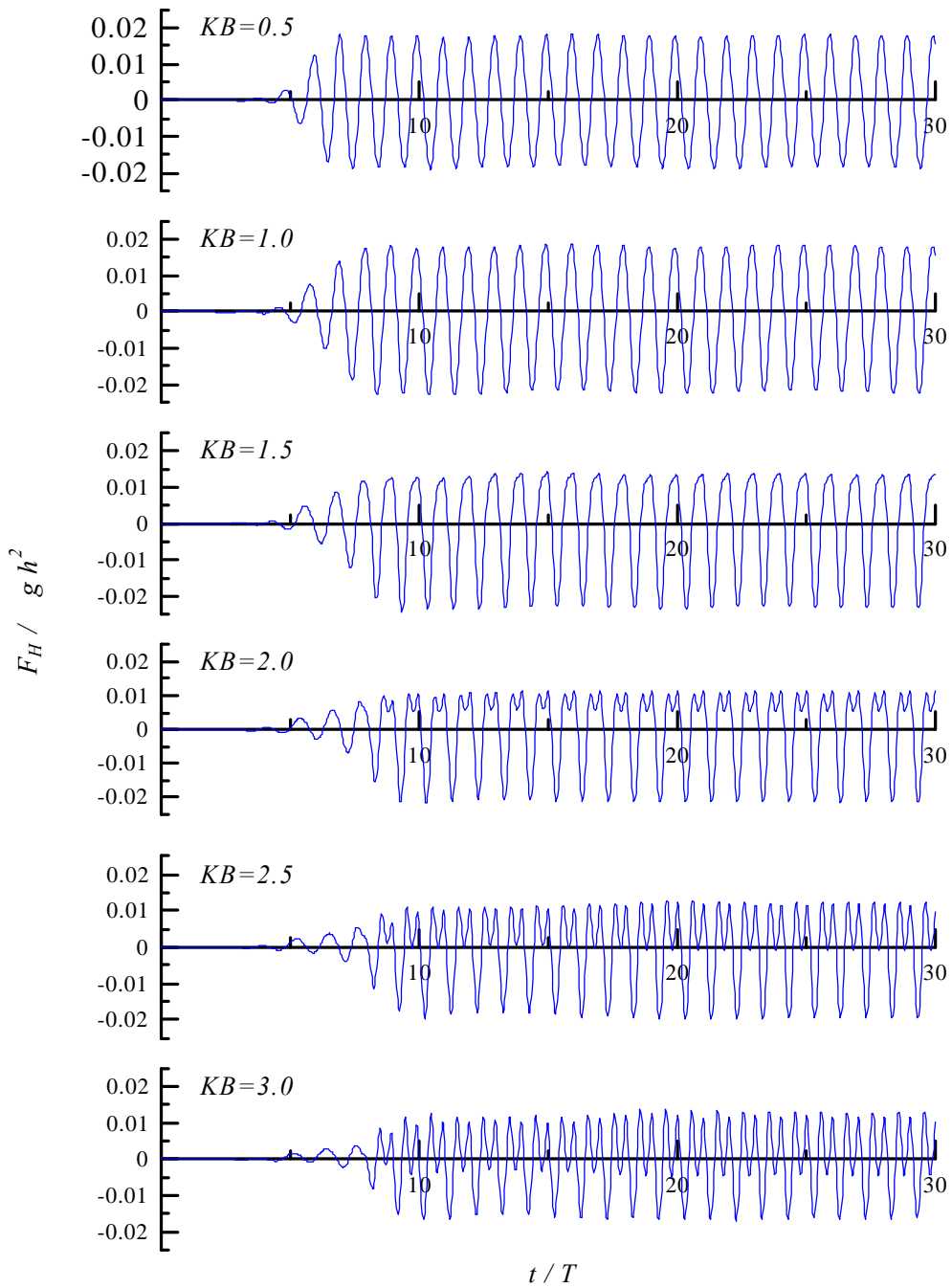


Fig.18 Simulated time series of heave exciting force acting on a fixed Lewis form body, $A/h = 0.035$.

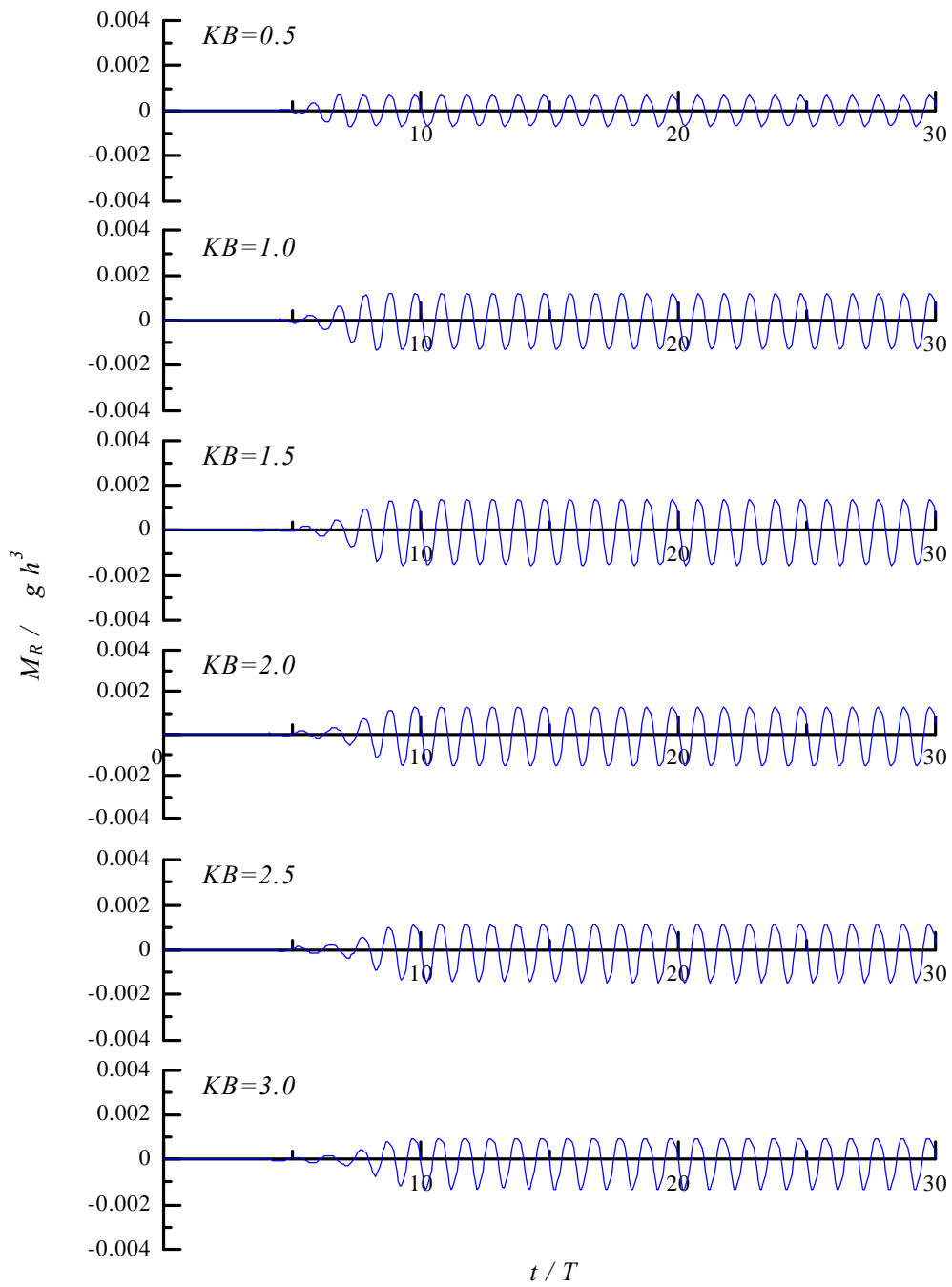


Fig.19 Simulated time series of roll exciting moment acting on a Lewis form body, $A/h = 0.015$.

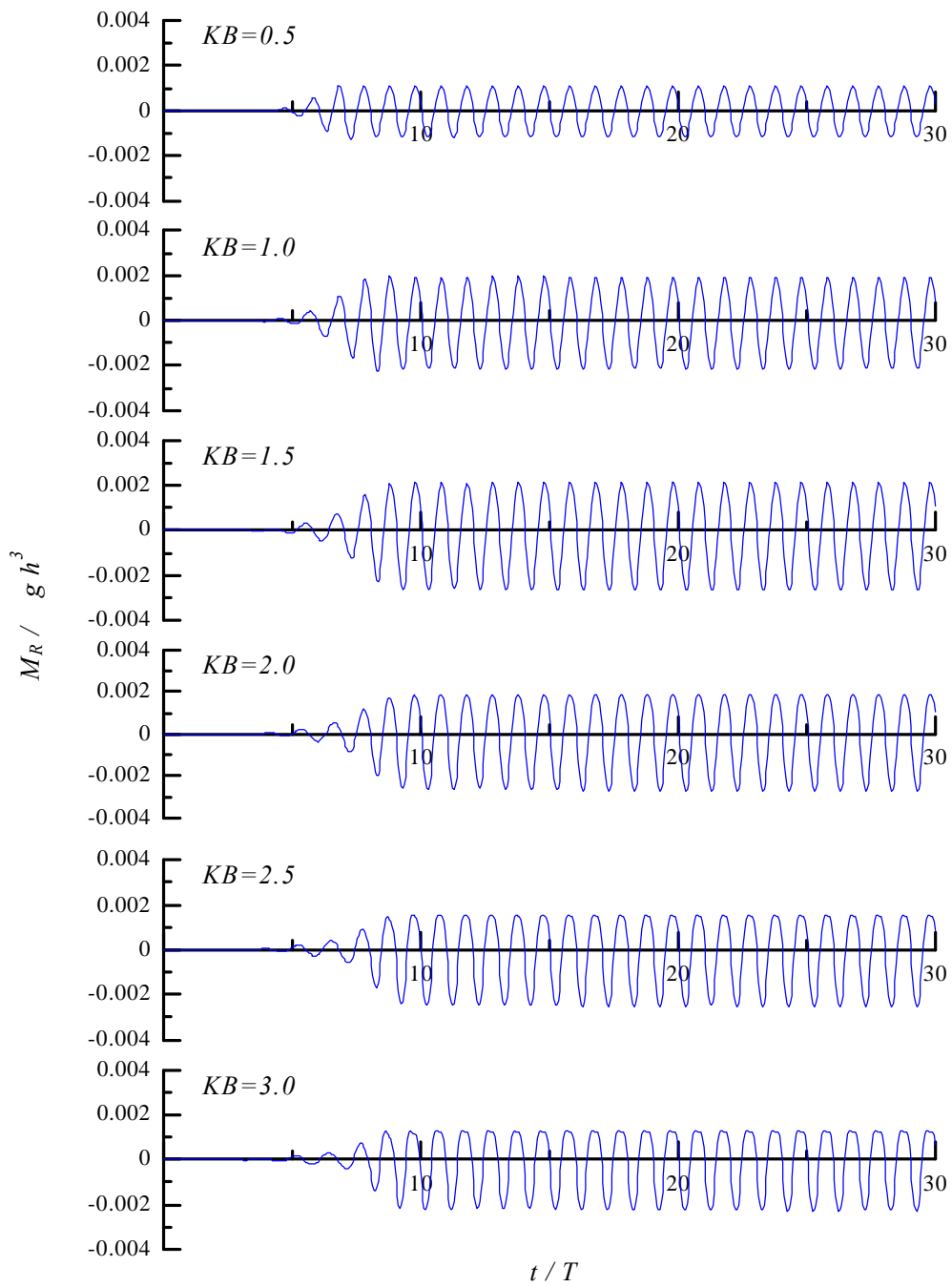


Fig.20 Simulated time series of roll exciting moment acting on a fixed Lewis form body, $A/h = 0.025$.

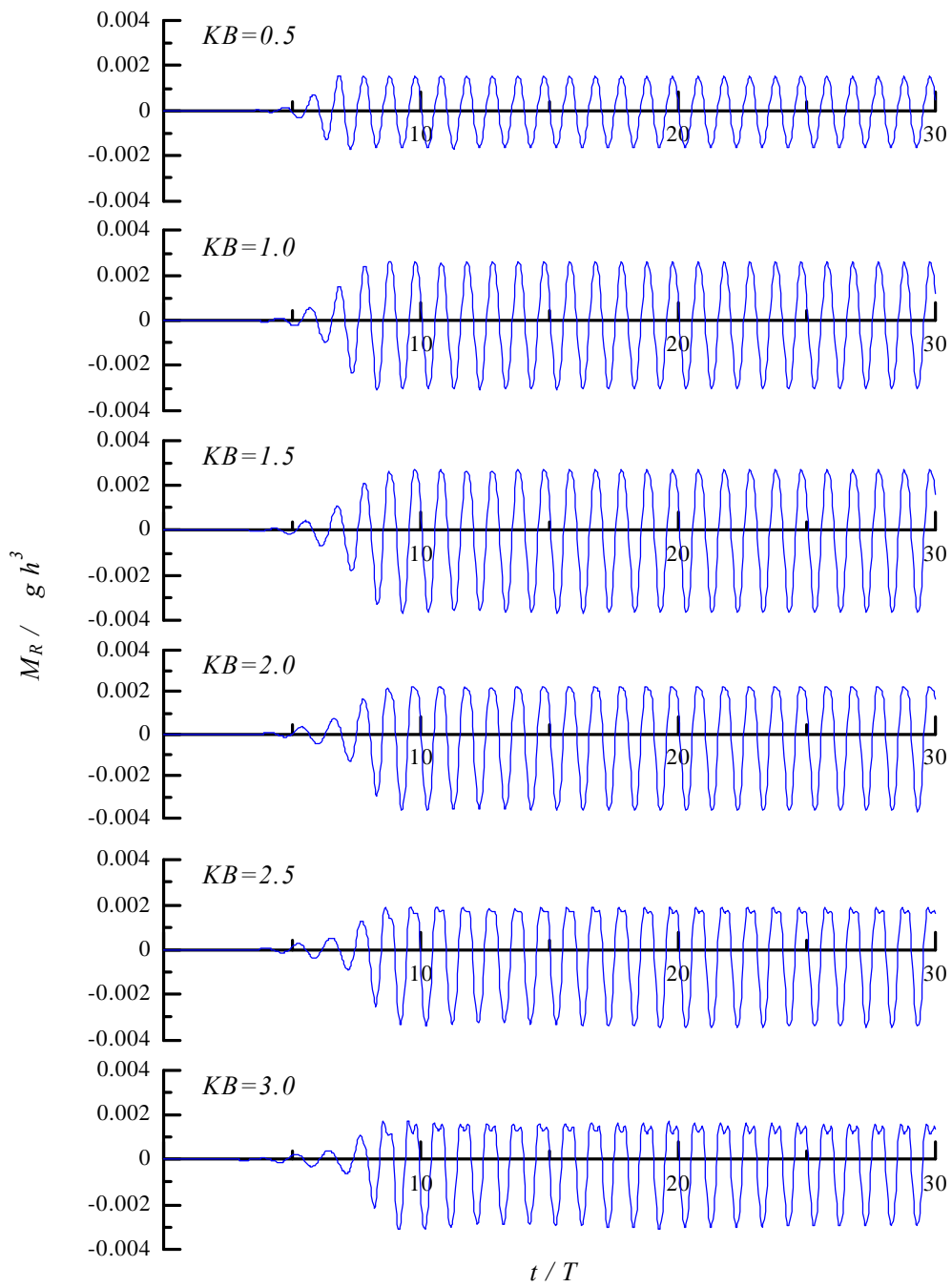


Fig.21 Simulated time series of roll exciting moment acting on a fixed Lewis form body, $A/h = 0.035$.

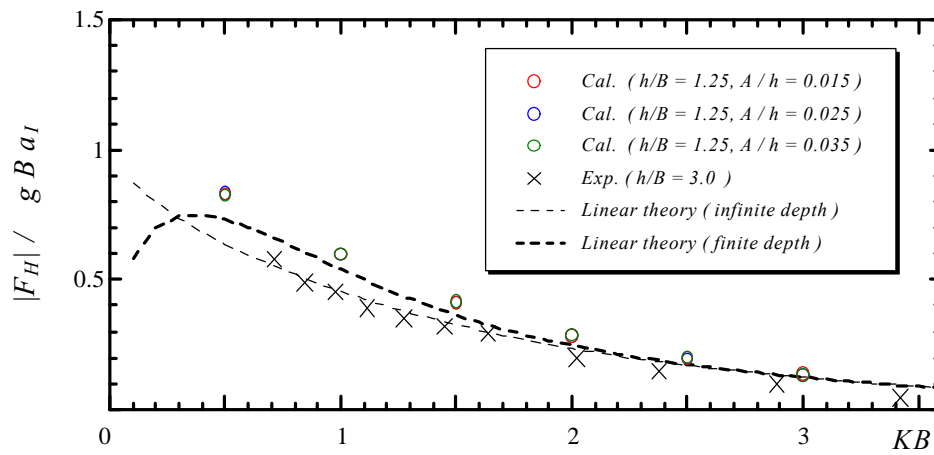


Fig.22 Heave exciting force acting on a fixed Lewis form body

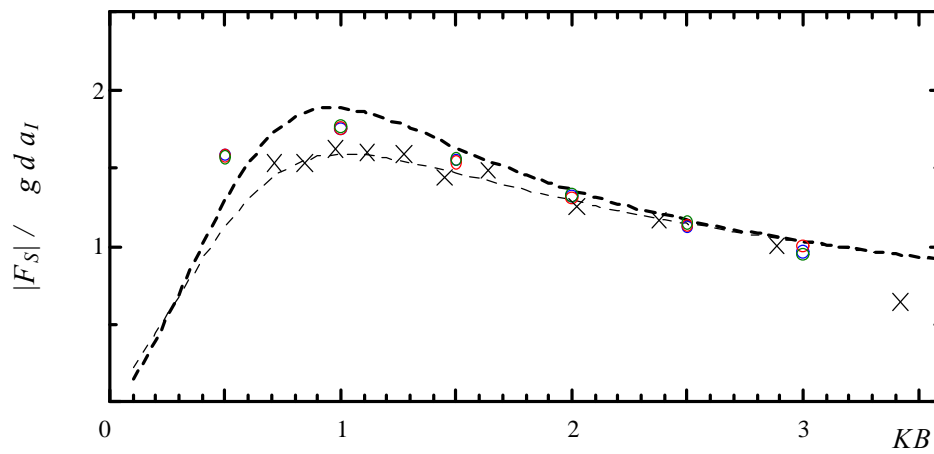


Fig.23 Sway exciting force acting on a fixed Lewis form body

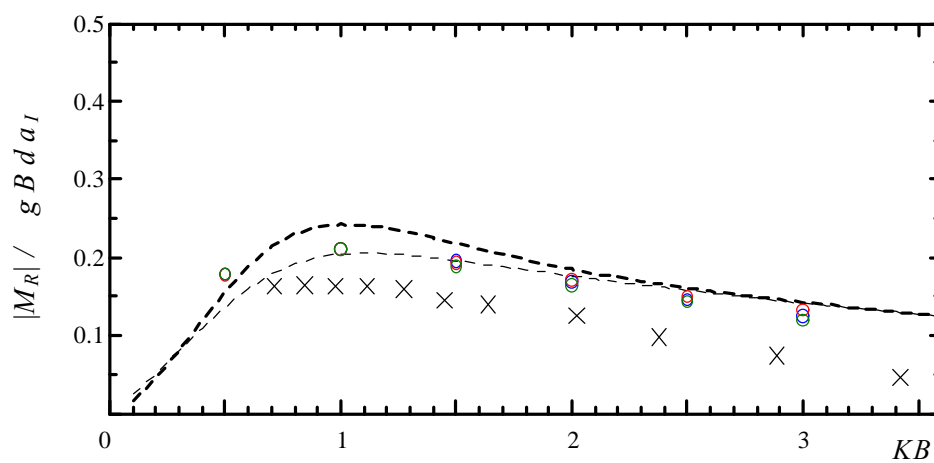
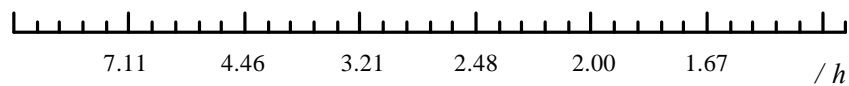


Fig.24 Roll exciting moment acting on a fixed Lewis form body



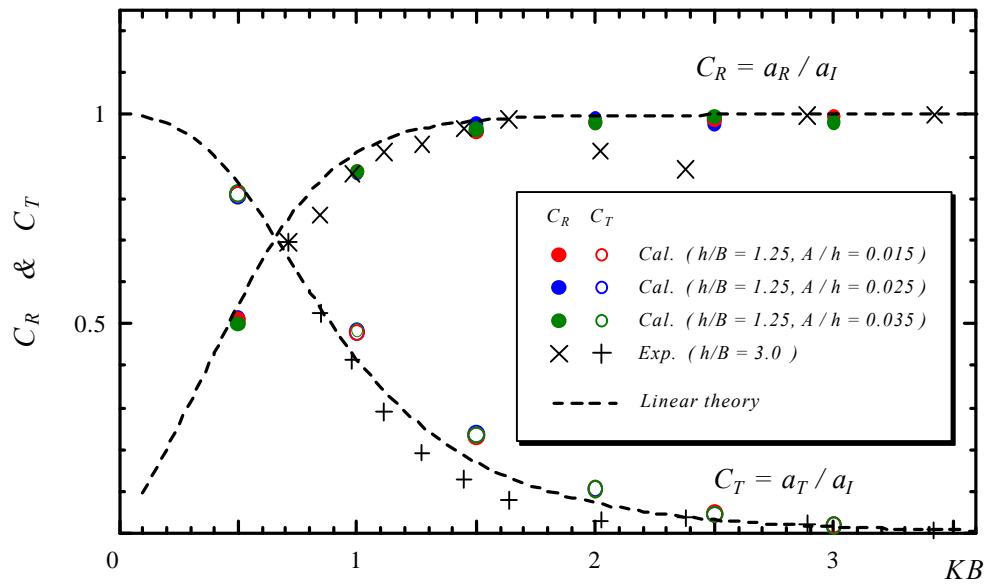


Fig.25 Reflection coefficient C_R and transmission coefficient C_T

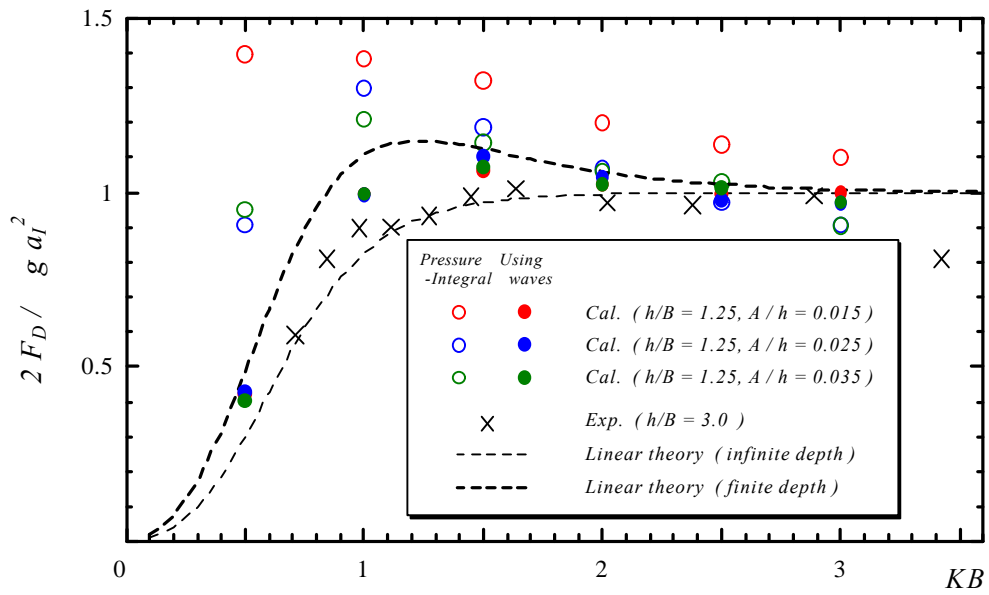


Fig.26 Wave-drift force acting on a fixed Lewis form body

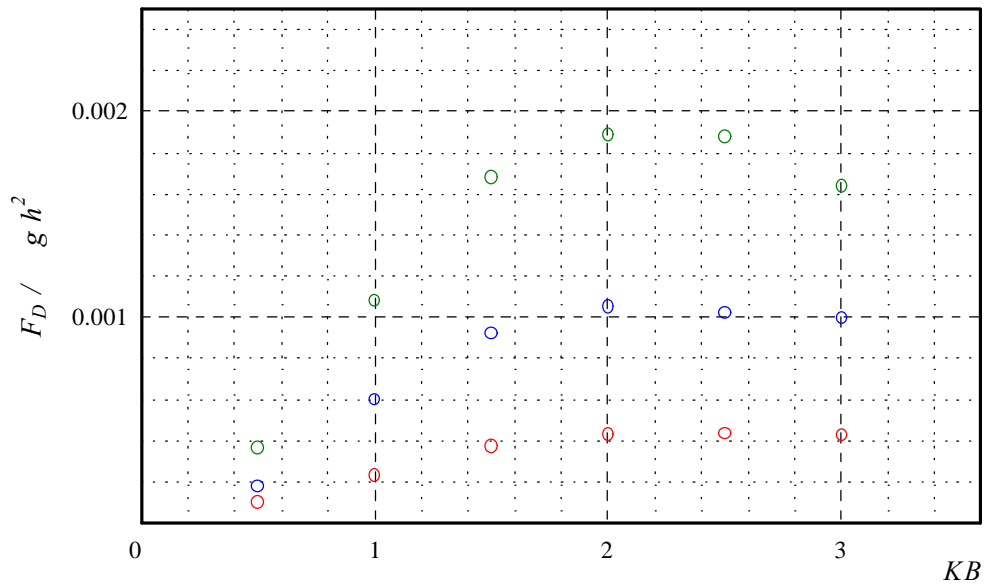


Fig.27 Wave-drift force computed by direct pressure integral

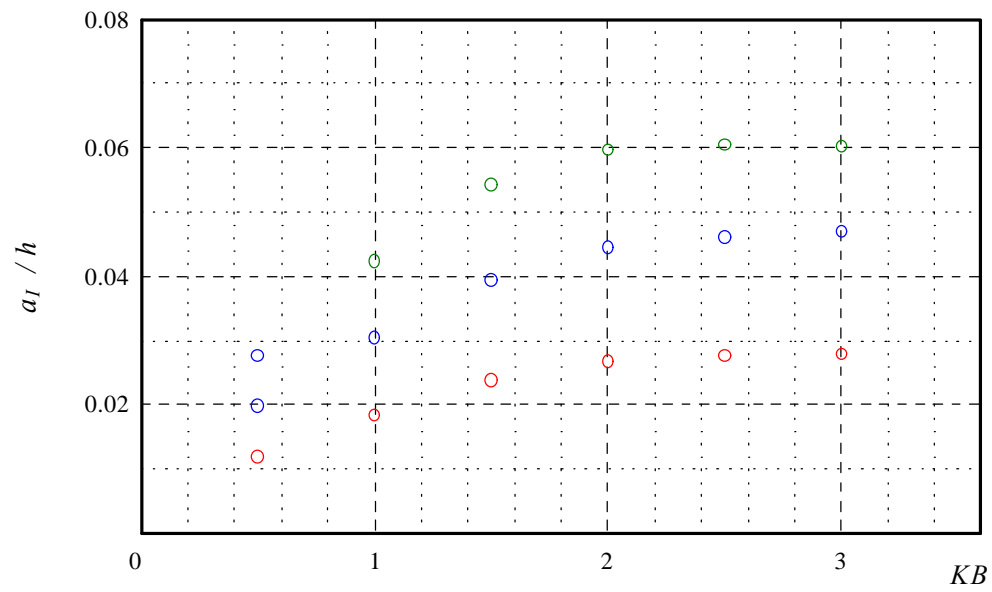


Fig.28 The amplitude of incident wave

4 Conclusions

The fully-nonlinear time domain simulation program is developed to predict the two dimensional diffraction loads by a fixed Lewis form body in regular waves. The computations by this numerical wave tank are performed to the diffraction problems with eighteen cases and compared with other computational results and experimental ones. The most important points highlighted in this numerical study are as follows:

- In the numerical wave tank whose length is 6 wave-length including wave absorbing zone of 2 wave-length, the stable solutions can be obtained from the rest until the periodically steady state.
- Considering the fundamental frequency component of the simulated wave-exciting forces acting a fixed Lewis form body, it shows good agreements with the prediction by linear theory. The effects of the wave height are not recognized for the first order wave-exciting force.
- The simulated wave-exciting force itself includes nonlinear properties in some cases, and the second harmonics becomes substantial especially in case of high frequency, even though the wave height is not so large.
- To apply the direct pressure integral method to predicting the wave-drift forces, the development of the numerical procedure with higher accuracy is needed. However, the present numerical wave tank can provide computational results enough to predict the first order wave-exciting forces. So it is also possible to predict the wave-drift forces by using these results about the first order's quantity.

The present fully-nonlinear Numerical Wave Tank based on the BEM, in which both velocity and acceleration field are solved, provides the fruitful computational results to predict the diffraction loads. Moreover the development of numerical procedure and present computer's performance make the computational time more practical. The objective evaluation to present results and the comparison with other procedures will be supplemented in the 3rd workshop of ISOPE 2000.

References

- Clement, A.H. (1997) *Dynamic Nonlinear Response of OWC Wave Energy Devices*, International Journal of Offshore and Polar Engineering, Vol.7, No.2, pp154-159.
- Cointe, R., Molin, B. and Nays, P. (1988) *Nonlinear and Second-Order Transient Waves in a Rectangular Tank*, Proc. of the Int. Conf. On Behavior of Offshore Structures, Trondheim, June, pp.705-719.
- Contento, G. (2000) *Numerical wave tank computations of nonlinear motions of two-dimensional arbitrarily shaped free floating bodies*, Ocean Engineering, Vol.27, No.5, pp.531-556.
- Daalen van, E.F.G. (1993). *Numerical and Theoretical Studies of Water Waves and Floating Bodies*, Ph.D. Thesis, University of Twente, The Netherlands.
- Grilli, S.T. , Skourup, J. and Svendsen, I.A. (1989) *An efficient boundary element method for nonlinear water waves*, Engineering Analysis with Boundary Elements, Vol.6, No.2, pp.97-107.
- Kihara, H. (1998) *Nonlinear Hydrodynamic Forces acting on Slender Body Ship in Large Amplitude Motion*, Ph.D. Thesis (Japanese), Osaka University, Japan.
- Nojiri, N and Murayama, K. (1975) *A Study on the Drifting Force on Two-Dimensional Floating Body in Regular Waves*, Trans. of West-Japan Soc. Naval Arch, Vol.51, pp.131-152.
- Oortmerssen van, G. (19) *The Interaction between a Vertical Cylinder and Regular Waves*, Technical report of Netherland Ship Model Basin, Wageningen, The Netherlands.
- Tanizawa, K. and Naito, S. (1998). *An Application of Fully Nonlinear Numerical wave Tank to the Study on Chaotic Roll Motions*, The Proc. of 8th International Offshore and Polar Engineering Conference, Vol. III, pp.280-287.